THE EFFECTS OF HYDROSTATIC TENSILE STRESS ON FRACTURE IN SOME STRUCTURAL ALLOYS

M. Shimura and S. Saito

The Research Institute for Iron, Steel and Other Metals, Tohoku University, Katahira-2, Sendai, Japan

ABSTRACT

Using Bridgman-type tensile specimens with natural necking profile, the characteristics of fracture in some structural alloys are shown to be co-related by the hydrostatic state of stress. The observations are summarized as failure maps which can express the characteristics of fracture of structural alloys as a curved surface divided by the dominance of micromechanism of fracture in three-dimensional space (fracture strain-temperature-hydrostatic tensile stress). In the case of ductile fracture, the strain to failure decreases as the hydrostatic tensile stress increases but the sensitivity varies from material to material. In the case of ferritic steel, ductile-brittle transition phenomenon is recognized depending on the hydrostatic tensile stress. In the case of cleavage fracture and intergranular fracture, there is also the dependency of the strain to failure on the hydrostatic tensile stress. A parameter x_o^c/δ_c, which could be a material constant (Rice and Sorensen, 1978), can be obtained by the superposition of failure locus in the map and the deformation history of point ahead of blunting crack.

KEYWORDS

Hydrostatic tensile stress; Failure maps; Ductile fracture; Cleavage fracture; Intergranular fracture; Ductile-brittle transition.

INTRODUCTION

Structural alloys are commonly deformed plastically under complex state of stress in the fabrication process and their subsequent structures are rarely used in simple stress state. Thus in order to design and use materials effectively in these conditions, it is necessary to be able to test and understand their behaviour in complex stress states. Recently, the mechanisms by which failure is initiated in small yielding and full plasticity are discussed with particular reference to microvoid nucleation, growth, and coalescence in multiaxial states of stress ahead of cracks in plane-strain conditions (Hancock and MacKenzie, 1976; Hancock and Cowling,1980). In addition, from the viewpoint of deformability of materials, a third mode of utilization of failure maps viz. the examination of the influence of stress state on the occurrence of a well defined and quantitatively characterized mode of fracture is required (Embury and LeRoy, 1978).

In this work the effects of hydrostatic tensile stress on fracture for some structural alloys are investigated in a convenient plastic flow field under the hydrostatic tensile stress (negative pressure, mean normal stress). Since the concerned papers have been already published (Shimura and Saito, 1980; Saito and Shimura, 1980; Saito, Shimura and Tanaka, 1980; Saito, Shimura and Tanaka, 1981), the test method and the failure map which summarizes the results of each alloy will be described concisely. The effect of hydrostatic tensile stress on various fracture modes and the application of the failure map for the estimation of the toughness of materials will also be described in this presentation.

EXPERIMENTAL PROGRAMME

Mechanical Testing

Bridgman-type tensile specimens with a natural necking profile after Dondik's equation (Dondik, 1970) were used in the convenient plastic flow field under the hydrostatic tensile stress. The results of Bridgman's analysis (Bridgman, 1952) have been used to obtain the values of the strain and the hydrostatic tensile stress component where failure occures. The main features of the analysis are that the strain is constant across the mean cross-section and this condition is satisfied by the natural necking profile (Argon and Im, 1975). The tensile tests have been performed in the condition of crosshead speed 0.5 mm/min.

Materials

Four ferritic steels and one titanium alloy and one high strength aluminum alloy have been tested. They are all representative practical structural alloys. Their chamical compositions are shown in Table 1.

TABLE 1 Chemical Composition (wt%)

	C	Si	Mn	P	S	Cu	Ni	Cr	V	Mo	Nb	O	N
S45C steel	0.45	0.24	0.82	0.021	0.023	0.01	0.01	0.03	-	-	-	-	-
S25C steel	0.24	0.21	0.42	0.016	0.019	0.04	0.01	0.02	-	-	-	-	-
SM50 steel	0.16	0.44	1.42	0.017	0.004	-	0.01	0.01	0.07	-	-	-	-
Ferritic stainless	0.002	0.14	0.05	0.020	0.010	-	0.17	30.3	-	1.90	0.10	0.002	0.006

	Si	Fe	Cu	Mn	Mg	Cr	Zn	Ti
7075 Aluminum alloy	0.07	0.21	1.60	0.01	2.60	0.19	5.60	0.01

	Al	V	Fe	N	O	H	C	Si
Ti-6Al-4V alloy	6.18	4.30	0.20	0.002	0.145	0.003	0.014	0.021

S25C and S45C are steels for mechanical structural parts and SM50 is a typical steel for welded structure. The ferritic stainless steel is one of the high-purity high-cromium steel. Ti-6Al-4V alloy is a typical, high strength titanium alloy and 7075 aluminum alloy is a high strength precipitation-hardened alloy. Fabrication histories of the alloys are shown in Table 2 and these processes are conventional.

TABLE 2 Processing of the Materials

Steels (S25C, S45C, SM50)
Ingot ---- Blooming ---- Hot Rolling ---- Normalizing

High-Purity Fe-30Cr-2Mo Alloy
Ingot ---- Blooming ---- Hot Forging

Ti-6Al-4V Alloy
Ingot ---- Hot Forging ---- Annealing

7075 Aluminum Alloy
Ingot ---- Homogenizing ---- Hot Rolling
T6, T73 - treatment

EXPERIMENTAL RESULTS, ANALYSIS AND DISCUSSION

Failure Maps of Commercial Structural Alloys

The informations from the tests are summarized in the way in Fig. 1. The axes are fracture strain, ε_f, temperature, T, and mean maximum hydrostatic tensile stress component along the deformation trajectory, normalized by flow stress, $(\bar{\sigma}_t/Y)$. The characteristics of failure of each alloy are shown as a curved surface in the three dimensional space. Open circles on the surface in Fig. 1 indicate that the fracture mechanism is overall fibrous fracture; double circles means bimodal (fibrous and cleavage) fracture; crossed circles denote overall cleavage fracture. Figure 1 shows failure maps for four ferritic structural steels. In all cases the curved surface is divided into three regions by fracture modes and it is suggested that the transition of fracture mode is dependent not only on temperature but also on hydrostatic tensile stress component. As seen in maps, the higher the hydrostatic tensile stress, the lower the fracture strain. Figure 2 is examples of failure map of the nonferrous structural alloy. Figure 2(b) shows a failure map for the Ti-6Al-4V alloy. As seen in the figure, the higher the hydrostatic tensile stress, the lower the fracture strain. Fracture surface of all specimens revealed the ductile mode and any transition of fracture mode was not found. Figure 2(a) shows a failure map for the 7075-T6 alloy. The alloy fails by intergranular mode.

Ductile Fracture

Interrelations between the fracture strain and the hydrostatic tensile stress are plotted on one-side logarithmic scale in the case of overall fibrous fracture of various alloys, as shown in Fig. 3, where the fracture strains are normalized by the fracture strains ε_f^o of unnotched tensile specimen. It was found that data on S25C steel, S45C steel, Ti-6Al-4V alloy and 7075-T73 aluminum alloy lay on straight lines and data on Fe-30Cr-2Mo alloy and SM50 lay on concave lines. On the whole, ductile fracture depends markedly on the stress state which may be characterized by σ_t/Y but the sensitivity varies from material to material. Void nucleation processes have been widely discussed. The dominant event leading to failure initiation in the structural alloys is void growth, as the formation of voids starts at very small strains. After nucleation the growth of microvoids has been established to depend on the state of stress. Rice and Tracey's analysis (1969) of the growth of an initially spherical void gave the rate-of-change of the mean void radius with plastic strain at high values of σ_t/Y. If it is assumed that the failure strain is inversely proportional to void grow-rate, then the failure strain can be expressed as

$$\varepsilon_f = \alpha \exp(-3\sigma_t/2Y) \tag{1}$$

where α is a material constant. The results shown in Fig. 3 illustrate the exponential relationship between ε_f and σ_t/Y. After failure initiation, deformation is largely confined to the growth of a central crack in the minimum cross-section. In this experiment, all specimens always failed at the centre. The volume fraction of voids for flow localization is expressed as a function of stress-state (Hancock and MacKenzie, 1976; Hancock and Cowling, 1980). This suggests that in very dirty materials at severe stress-states, flow localization may occur as soon as the voids are formed.

Cleavage Fracture

Interrelations between the fracture strain and the hydrostatic tensile stress are shown in the case of overall cleavage fracture of various ferritic structural steels, as shown in Fig. 4. In each case, the fracture strain decreases with the increase of hydrostatic tensile stress but the dependency of the fracture strain on hydrostatic tensile stress varies from material to material. The critical stress level for cleavage is reached by a contribution from the hydrostatic component of the stress state and a strain-hardening component from effective stress. Thus, when hydrostatic tensile stress is high, the critical stress level can be reached at lower plastic strain. When the cleavage crack is crossing the grain boundary, its propagation is prevented. The stress needed at this stage can be calculated simply by using the Griffith formula (Francois, 1977);

$$\sigma_F - p = \left[\frac{\pi E \gamma_B}{(1-\nu^2)4d}\right]^{1/2} \tag{2}$$

where γ_B is the fracture energy for crossing the grain boundary, p is pressure and d is the grain size. If the pressure is negative viz. hydrostatic tensile stress is operating, the fracture stress decreases with the increase of negative pressure.

Ductile-Brittle Transition

The region where the double circles are distributed in the failure maps (Fig. 1) is ductile-brittle transition region. The cleavage mechanism of fracture is always in competition with the ductile mechanism in the transition region. In this region, ductile fracture starts at the centre in the minimum cross-section and then the ductile crack grows radially and subsequently change to cleavage. In the case of high hydrostatic tensile stress state, deformation after failure initiation is localized to a thin disc region in the minimum cross-section and results in the flat fracture surface perpendicular to the tensile axis. Figure 5 shows area fraction (%) of cleavage part for overall fracture surface in the case of bimodal fracture.

It is suggested that the ductile-brittle transition occurs at early time (namely, in the case of small ductile crack) under high hydrostatic tensile stress state. The effect of the prior deformation plus the sudden increase in triaxiality raise the stress level to that for cleavage and cause a fracture mode transition. Figure 6 shows relationships between the fracture strain and the hydrostatic tensile stress in the case of bimodal fracture. It seems probable that hydrostatic tensile stress influences directly the tensile stress-opereted cracking and affects to an upward shift in the ductile-brittle transition temperature.

Intergranular Decohesion

The intergranular decohesion was dominant in the case of 7075-T6 aluminum alloy. The relationships between the fracture strain and the hydrostatic tensile stress are plotted on one-side logarithmic scale, as shown in Fig. 7. In this case, the fracture strain decreases with the increase of the hydrostatic tensile stress but the relationship is not a simple exponential relation as in the case of overall fibrous fracture. Intergranular cracks occur parallel to the tensile axis in 7075-T6 aluminum alloy samples which were fractured under hydrostatic tensile stress. In this case the pan-cake structure from the hot rolling plays an essential role.

APPLICATION OF FAILURE MAPS FOR THE ESTIMATION OF TOUGHNESS

By following the large geometry change involved in blunting Rice and Johnson (1970) presented both the triaxiality (σ_t/Y) and effective plastic strain $\bar{\varepsilon}^p$ as functions of x_o/δ, where x_o is the original distance of a point from the initially sharp crack tip and δ is crack opening displacement. The volume of material that is subject to critical strains, stresses, or a combination of both also increases until eventually sufficient material is encompassed for the appropriate fracture mechanism to operate and the crack to extend. On the other hand the essential feature in axisymmetric tensile specimens is that the plastic strain to initiate failure $\bar{\varepsilon}^p_f$ is a function of the triaxiality. Thus, a parameter x_o/δ is to be obtainable by the superposition of failure locus in the failure map and the deformation history ahead of a crack tip. Figure 8 shows the superposition of Rice-Johnson deformation history and failure loci for the structural alloys at room temperature. Each point of intersection on these trajectories corresponds to a value of x_o^c/δ_c which can be deduced by returning to the original data. According to Rice and Sorensen (1978) x_o^c/δ_c is a material constant which is directly related to the toughness of material. Figure 9 shows the experimental values of x_o^c/δ_c of the structural alloys determined in the wide range of temperature. The temperature sensitivity of the parameter is low in 7075 aluminum alloy and Ti-6Al-4V alloy, while the parameters in the ferritic structural steels increase with the decrease of temperature.

REFERENCES

Argon, A. S. and J. Im (1975). Met. Trans., 6A, 839-851.

Bridgman, P. W. (1952). Studies in Large Plastic Flow and Fracture. McGraw-Hill, New York.

Dondick, I. G. (1970). Problemy Prochnosti, No. 8, 54-56.

Dondick, I. G. (1972). Strength of Materials, 937-940.

Embury, J. D. and G. H. LeRoy (1978). Fracture 1977, ICF4, Vol. 1, pp. 15-42.

Francois, D. (1978). Fracture 1977, ICF4, Vol. 1, pp. 805-820.

Hancock, J. W. and A. C. MacKenzie (1976). J. Mech. Phys. Solids, 24, 147-169.
Hancock, J. W. and M. Cowling (1980). Metal Sciences, 14, 293-304.
Rice, J. R. and D. M. Tracey (1969). J. Mech. Phys Solids, 17, 201-217.
Rice, J. R. and M. A. Johnson (1970). In M. Kanninen (Ed.), Inelastic Behaviour of Solids, McGraw-Hill, 641-672.
Rice, J. R. and E. P. Sorensen (1978). J. Mech. Phys. Solids, 26, 163-186.
Saito, S. and M. Shimura (1980). Proc. 4th Int. Conf. Ti, pp. 1685-1689.
Saito, S., M. Shimura and E. Tanaka (1980). Tetsu-to-Hagane (J. Iron and Steel Inst. Japan), 66, 1650-1658.
Saito, S., M. Shimura and E. Tanaka (1981). Keikinzoku (J. Japan Inst. Light Metals), 31, 455-461.
Shimura, M. and S. Saito (1980). The Science Reports of the Research Institutes, A-Vol. 29, Tohoku University, 50-69.

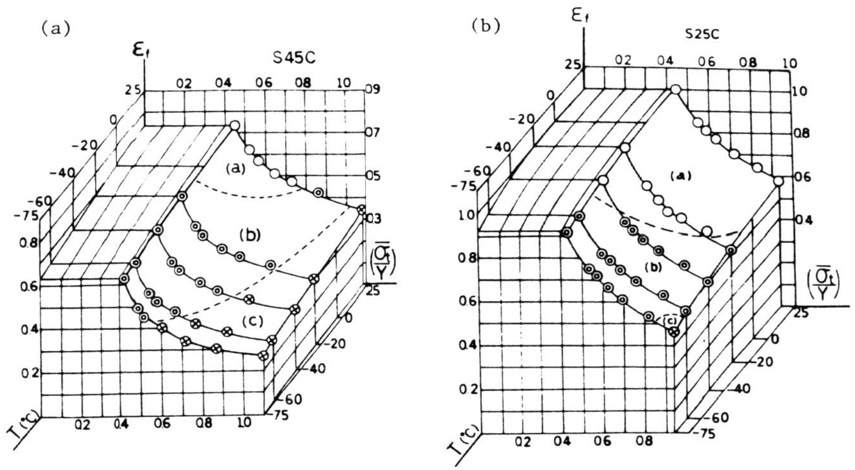

Fig. 1. Failure maps for ferritic structural steels.
(a) S45C steel, (b) S25C steel.
○ : Overall fibrous fracture, ◎: Bimodal fracture, and
⊗ : Overall cleavage fracture.

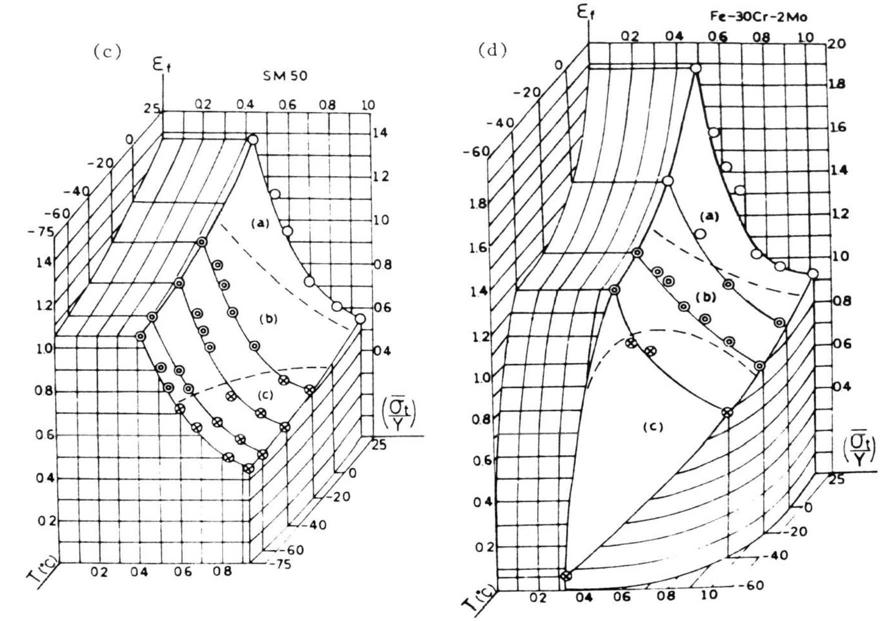

Fig. 1. Failure maps for ferritic structural steels.
(c) SM50 steel, (d) Fe-30Cr-2Mo stainless steel.
○: Overall fibrous fracture, ◎: Bimodal fracture, and
⊗: Overall cleavage fracture.

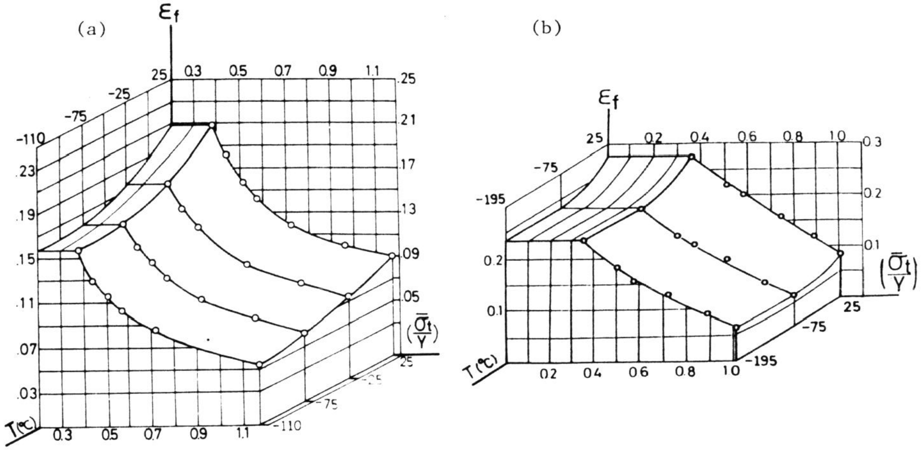

Fig. 2. Failure maps for non-ferrous structural alloys.
(a) 7075-T6 aluminum alloys, (b) Ti-6Al-4V alloy.
●: Transgranular fracture, ○: Overall fibrous fracture.

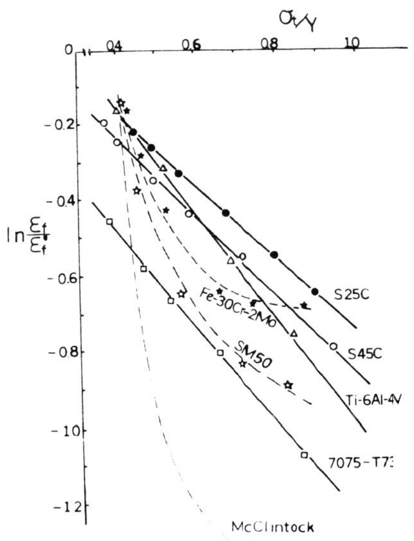

Fig. 3. Relationships between fracture strain and hydrostatic tensile stress in the case of overall fibrous fracture.

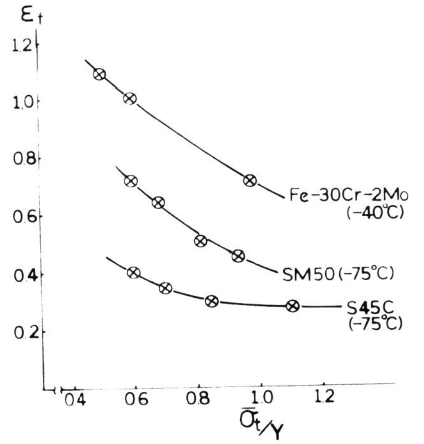

Fig. 4. Relationships between fracture strain and hydrostatic tensile stress in the case of overall cleavage fracture.

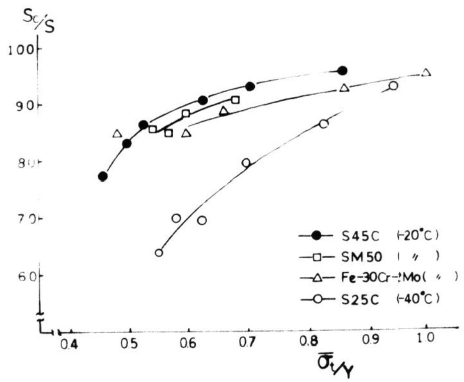

Fig. 5. Relationships between hydrostatic tensile stress and area fraction (%) of cleavage region in whole fracture surface in tha case of bimodal fracture.

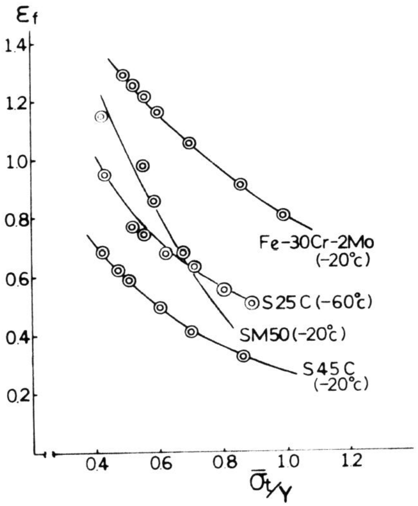

Fig. 6. Relationships between fracture strain and hydrostatic tensile stress in the case of bimodal fracture.

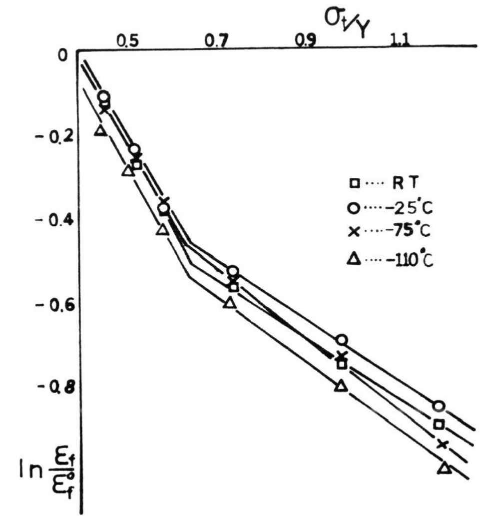

Fig. 7. Relationships between fracture strain and hydrostatic tensile stress in the case of intergranular fracture of 7075-T6 aluminum alloy.

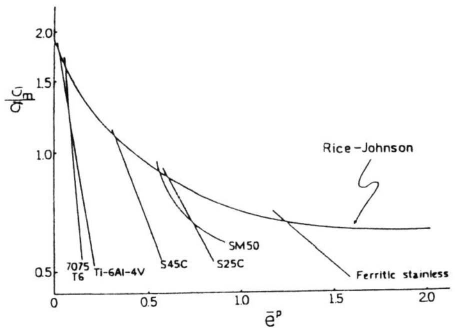

Fig. 8. Superposition of Rice-Johnson deformation history and failure loci for structural alloy in room temperature.

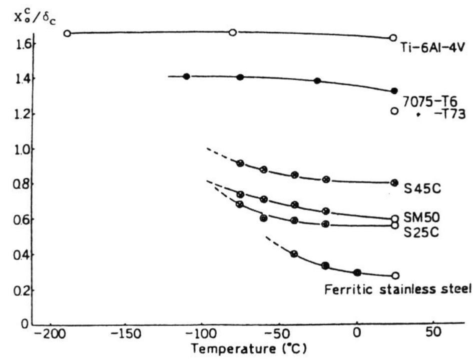

Fig. 9. Characteristic parameter x_o^c/δ_c versus temperature for some structural alloys.